Journal of Power Sources 206 (2012) 210–214

Contents lists available at SciVerse ScienceDirect

Journal of Power Sources

journal homepage: www.elsevier.com/locate/jpowsour

Short communication

Characteristics and performance improvement of anode supported solid oxide fuel cells based on $BaIn_{0.3}Ti_{0.7}O_{2.85}$ (BIT07) as electrolyte, BIT07-Ni as anode and $La_{0.58}Sr_{0.4}Co_{0.2}Fe_{0.8}O_{3-\delta}$ (LSCF) as cathode

M. Letilly, O. Joubert, A. Le Gal La Salle*

Institut des Matériaux Jean Rouxel (IMN), CNRS-Université de Nantes, 2 rue de la Houssinière, BP 32229, 44322 Nantes, France

ARTICLE INFO

Article history:
Received 24 August 2011
Received in revised form 23 January 2012
Accepted 24 January 2012
Available online 1 February 2012

Keywords:
BIT07
SOFC
Tape casting
Screen-printing
Cell test
EIS

ABSTRACT

This study deals with the electrochemical performance of anode supported solid oxide fuel cells (SOFCs) based on perovskite-type materials: $BaIn_{0.3}Ti_{0.7}O_{2.85}$ (BIT07) as electrolyte, BIT07-Ni as a cermet anode and $La_{0.58}Sr_{0.4}Co_{0.2}Fe_{0.8}O_{3-\delta}$ (LSCF) as cathode. Anode/electrolyte assemblies have been realised by tape casting and co-firing and the cathode has been deposited by screen-printing. The performance of BIT07-Ni/BIT07/LSCF cells has been determined at 700 °C under humidified (3% H_2O) hydrogen as fuel and air as oxidant. Two cells, with different electrolyte thicknesses: 23 and 11 μm, have been tested and they exhibited power densities at 0.7 V around 209 and 336 mW cm^{-2}, respectively. Electrochemical Impedance Spectroscopy (EIS) measurements have also been carried out and allowed to differentiate between the series and polarisation resistances.

1. Introduction

Solid oxide fuel cells (SOFCs) are all-solid devices converting the chemical energy of gaseous fuels, such as hydrogen or natural gas, into electricity, via electrochemical processes and presenting advantages such as high energy conversion efficiency, low greenhouse gas emission, or flexibility of fuels [1]. At high operating temperatures (800–1000 °C), several issues are encountered (use of expensive ceramic interconnectors and stability of the cell) and thus lowering the working temperature of SOFC around 600–800 °C is necessary [2].

Due to its intrinsic properties, such as its conductivity level at 700 °C, its stability under a large oxygen partial pressures range and its stability under CO_2 atmosphere, it has been demonstrated in previous papers that $BaIn_{0.3}Ti_{0.7}O_{2.85}$ (BIT07) is a suitable electrolyte material for SOFC [3,4].

Tape casting is one of the most used design techniques for SOFC components, as it is cost-efficient and easy to up-scale to mass production [5] and by this method, anode/electrolyte half-cells can be designed by multi-layer tape casting [6].

It has been first published that several steps are necessary to get a dense BIT07 electrolyte: (i) first the synthesis of the ceramic powder (two 24-h-thermal treatments: the first one at 1200 °C and the second one at 1350 °C) [4], (ii) then the reduction of the grain size (to obtain a submicron powder) to facilitate the sintering (the powder is ball-milled for 60 h at 500 rpm) and (iii) finally the sintering treatment (1300 °C for 9 h) [7].

BIT07 can also be used in a cermet anode combined with nickel since neither Ni nor NiO react with BIT07. Symmetrical anode/electrolyte/anode cells have thus been prepared by tape casting and co-firing. By varying the grain size of BIT07 powders, the BIT07/NiO ratio, the use of pore-forming agents, numerous anode compositions have been tested, and a minimal ASR value of 0.15 Ω cm^2 was finally obtained at 700 °C under wet (3% H_2O) Ar/H_2 (95/5) atmosphere for a cermet anode BIT07-Ni, realised with BIT07 and NiO in a 50:50 wt. ratio, and 5 wt.% carbon black (CB) as pore-forming agent [7].

It has also been demonstrated that BIT07 can be used with well-known cathode materials, such as $La_{0.7}Sr_{0.3}MnO_{3-\delta}$ (LSM), $La_{0.58}Sr_{0.4}Co_{0.2}Fe_{0.8}O_{3-\delta}$ (LSCF) or $Nd_2NiO_{4+\delta}$, and that best results regarding electrochemical performance have been obtained with LSCF [8]. This can be attributed to the self-induced formation of an accommodating layer of formula $Ba_xLa_{0.58(1-x)}Sr_{0.4(1-x)}In_{0.3x}Ti_{0.7x}Co_{0.2(1-x)}Fe_{0.8(1-x)}O_{3-\delta}$, with $0 \leq x \leq 1$ at the electrolyte/cathode interface [9]. It has been shown that this layer is not resistive, in contrary to what is observed between LSCF and the usual YSZ electrolyte [10–12], and allows an excellent match between the electrolyte and cathode, with

* Corresponding author. Tel.: +33 240373913; fax: +33 240373995.
E-mail address: annie.legal@cnrs-imn.fr (A. Le Gal La Salle).

0378-7753/$ – see front matter © 2012 Elsevier B.V. All rights reserved.
doi:10.1016/j.jpowsour.2012.01.138

mechanical and electrochemical properties varying from the electrolyte and cathode, as it is the case of graded or multi-layered electrodes [13,14] and avoiding thermal expansion coefficient mismatch between cathode and electrolyte [15,16]. By screen-printing LSCF onto BIT07 dense pellets and performing an appropriate heat treatment, it is possible to obtain reproducible LSCF/BIT07/LSCF symmetrical cells with interesting electrochemical properties such an ASR value of 0.07 Ω cm^2 at 700 °C [17].

Given the promising performance obtained on both anode and cathode symmetrical cells, complete Ni-BIT07/BIT07/LSCF cells have been realised by tape casting and screen printing. In this publication, they have been tested under air on the cathode side and wet H_2 (3% H_2O) on the anode side. Good performance have been achieved and discussed in terms of total resistance determined from current density/voltage curve (J/U) and Electrochemical Impedance Spectroscopy (EIS) measurements at the Open Circuit Voltage (OCV) to understand the origin of this resistance, and to determine the relevant parameters that can be modified in order to minimise it. The stability of the cell presenting the highest performance has been studied at the operating temperature of 700 °C.

2. Materials and methods

2.1. Powders

BIT07 was synthesised as detailed in [4]: its constituents, high purity barium carbonate (Alfa Aesar), indium oxide (Alfa Aesar) and titanium dioxide (Merck), in stoichiometric ratio, were mixed in mortar and pestle using alcohol. The mixture was first heated at 1200 °C for 24 h, then ground and compacted into a pellet of 40 mm diameter. This compact was then heated at 1350 °C for 24 h, ground and passed through mesh 100. LSCF powder (d_{90} = 50 μm) was provided by Marion Technologie and nickel oxide powder (grain size 0.5–1 μm) was provided by Pharmacie Centrale de France.

2.2. Cell fabrication

Prior to the cell fabrication in order to decrease their large grain sizes, powders have been ball-milled at 500 rpm: 60 h for BIT07 [7] and 4 or 15 h for LSCF [17]. The anode composition has been optimised to reach the best electrochemical performance, obtained with a BIT07-Ni cermet (BIT07:NiO 50:50 wt.%), realised with a BIT07 powder ball-milled for 60 h at 500 rpm and 5 wt.% CB as pore forming agent [7].

Fig. 1 presents the simplified flow-sheet for the complete cell preparation. The button cell (Ø 10 mm) is composed of an anode supported electrolyte/anode half-cell, prepared by tape casting and co-fired. Then a LSCF cathode (Ø 5 mm) is deposited on the electrolyte by screen-printing.

Two cells have been realised: named A and B. They both exhibit the same anode (which composition is given above). The two cells are different in terms of electrolyte thickness and cathode grain size. On one hand, cell A is made of an electrolyte tape cast at 100 μm and of a cathode realised with LSCF powder ball-milled for 4 h. And on the other hand, cell B is made of an electrolyte tape cast at 50 μm and of a cathode realised with LSCF powder ball-milled for 15 h. The influence of these two parameters: (i) electrolyte thickness after sintering (which is directly linked to the as-cast electrolyte thickness) and (ii) the cathode grain size (which is directly linked to the ball-milling duration of the LSCF powder), on the cell performance will be discussed later.

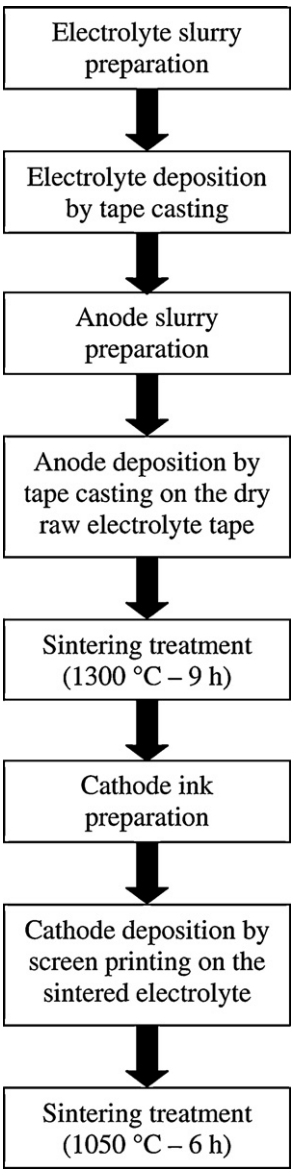

Fig. 1. Flow-sheet for the complete cell preparation.

2.3. Cell test

Current collectors, made of discs (5 mm in diameter) of gold grid (Goodfellow, AU008710, nominal aperture: 250 μm, wire diameter: 60 μm) are attached on both the electrodes using gold ink. The cell is placed at 130 °C for one night to evaporate the solvents and to obtain good electrical contacts. The current–voltage characteristic is measured with the use of a laboratory-made testing system [4]. The button cell was sealed (Aremco sealing material #571) on the top of an alumina sample tube (outer Ø 10 mm, inner Ø 6 mm) thus separating the atmospheres between the inside and outside of tube. The fuel-gas supply tube is situated inside the sample tube. The system was kept vertically in a tubular furnace. The measurements of current density (J) and voltage (U) were done by digital multimeters Keithley 197 and Protek 506, respectively. Current drawn in the circuit was varied using a rheostat. Effective area of the cells in this study was 0.2 cm^2 (cathode surface). Prior to the measurements, nickel oxide is reduced in situ at 700 °C for 2 h under wet H_2 and measurements were made at 700 °C, under wet (3% H_2O) H_2 on the anode side, and air on the cathode side.

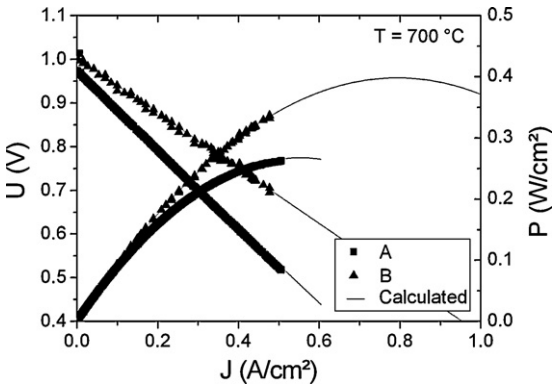

Fig. 2. Voltage and power density versus current density characteristics of the cells (■, A; ▲, B and –, calculated) recorded at 700 °C under wet (3% H_2O) hydrogen on the anode side and air on the cathode side.

Cells have also been tested by electrochemical impedance spectroscopy. The spectra have been recorded at OCV, with a signal amplitude of 0.1 V and with 84 points scattered in a frequency range from 65 kHz to 0.01 and 10 Hz for cell A and B, respectively, with a frequency response analyser Solartron 1255. It has been checked that the amplitude of the perturbation signal is small enough to meet the linearity requirement of the transfer function [18]. The data acquired from the impedance testing were analysed using ZView2-Software [19].

2.4. Post mortem analysis

Post mortem (after measurements) analyses of the cells have been carried out by SEM, using a JEOL 7600.

3. Results and discussion

3.1. Cells' performance

3.1.1. Characteristics' measurements

Fig. 2 presents the voltage (U) and power density (P) versus current density (J) characteristics obtained for the two cells A and B at 700 °C. In both cases, the polarisation curves (U/J) are clearly linear in the studied current density range. This polarisation curves provide open circuit voltage (OCV) and area specific resistance ($ASR_{(U/J)}$) of the cell, following the relation:

$$U = \mathrm{OCV} - \mathrm{ASR}_{(U/J)} \cdot J \quad (1)$$

The experimental set-up does not allow to obtain a current density high enough to get the maximum power density (named P_{max}) developed by the cell. Thus, the extrapolated U/J and P/J characteristics have been plotted (lines in Fig. 2) by using Eq. (1) and assuming that the U/J dependence is linear up to 0.6 and 1 A cm^{-2} for cell A and B, respectively.

3.1.2. Electrochemical measurements

Fig. 3 presents the Nyquist diagrams obtained for the two cells at 700 °C under wet (3% H_2O) hydrogen on the anode side and air on the cathode side. The diagrams are not well defined but however the ASR of the cells can be obtained and it is also possible to differentiate between the series and polarisation resistances, named R_s and R_p, respectively, which are related to the experimental set-up and the electrolyte (R_s) and the electrodes (R_p).

3.2. Post mortem analysis

Fig. 4 presents the *post mortem* SEM images of the cross-section of each cell. The cells have not been damaged by the measurement; no crack can be seen on the electrolyte; the anode and the cathode microstructures still present porosity. Moreover with those images the electrolyte thickness (named t) will be determined.

3.3. Discussion

Table 1 gathers the cells characteristics at 700 °C obtained from (i) the voltage and power density versus current density characteristics, (ii) the Nyquist diagrams of the complete cells and (iii) the SEM images.

In both cases, the OCV is lower than the theoretical value expected at 700 °C (1.125 V), suggesting a small leakage between gas chambers [4]. The power densities at 0.7 V are of about 209 and 336 mW cm^{-2} for cells A and B, respectively. The extrapolated maximum power densities (obtained by extrapolating the experimental J–U curves and represented by black line in Fig. 2), are of about 266 and 398 mW cm^{-2} for cells A and B, respectively. The ASR values obtained from the EIS measurements (0.91 and 0.68 Ω cm^2 for cells A and B, respectively) are in agreement with the ones obtained from the U/J curves (0.87 and 0.63 Ω cm^2 for cells A and B, respectively). Those values, obtained with a new electrolyte material, are promising even if they are not yet as good as the best ones found in the literature (see Table 2).

The detail of the $ASR_{(EIS)}$ shows that for the two cells the polarisation resistances, i.e. the part of the resistance due to electrode contribution, are equivalent (around 0.38 Ω cm^2), suggesting similarities of the anodes' and cathodes' contributions. This can be explained by the fact that (i) the two anodes are the same for the two cells, and (ii) it has been seen that the grain size of the cathode material (e.g. the ball-milling duration of 4 or 15 h) has only a small effect on the cathode contribution, which is always comprised between 0.07 and 0.15 Ω cm^2 (published elsewhere [17]), so the cathodes' contributions are comparable for the two cells. However a difference is seen concerning the series resistance, which is of 0.53 and 0.3 Ω cm^2 for cells A and B, respectively. This contribution is assimilated to the electrolyte contribution and the set up connections. It has been seen on the SEM images the two electrolytes are dense (Fig. 4), but their thickness are different by a factor of 2: 23 and 11 μm for cells A and B, respectively. This was expected given to the as-cast thickness: 100 and 50 μm for cells A and B, respectively (see Section 2.2). The difference of electrolyte thickness can explain the difference of series resistance. Assuming that the resistance from the set-up is negligible, the electrolyte conductivity can be calculated by using the following formula:

$$\sigma_{(\mathrm{electrolyte})} = \frac{t}{R_s} \quad (2)$$

Conductivity values of around 4.3×10^{-3} and 3.7×10^{-3} S cm^{-1} have been obtained for cells A and B, respectively. These values are far from the one obtained previously on a dense (95%) pellet realised with the same BIT07 powder (ball-milled for 60 h at 500 rpm) which was of 10^{-2} S cm^{-1} [7]. The difference observed between the expected and calculated conductivity values can be attributed to the current collection which adds a contribution to the series resistance value, those current collection issues are well described in the literature [24–26]. To improve the current collection the addition of LSC [27,28] and Ni deposits [29,30] on the cathode and the anode, respectively appears to be useful.

3.4. Ageing behaviour

The electrochemical behaviour of cell B has been followed with the time, during a few days (92 h) at the working temperature of 700 °C (Fig. 5). The cell has been placed at 0.7 V and its characteristics have been recorded every 24 h approximately.

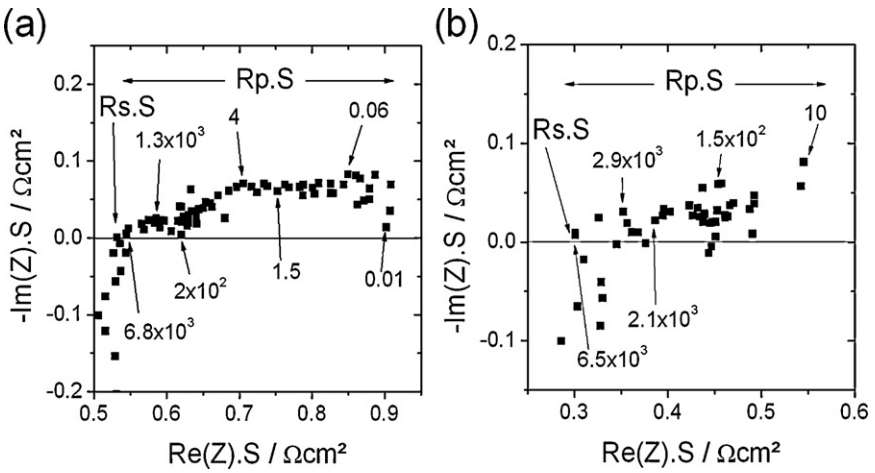

Fig. 3. Nyquist diagrams of the complete cells recorded at 700 °C under wet (3% H_2O) hydrogen on the anode side and air on the cathode side: (a) A and (b) B.

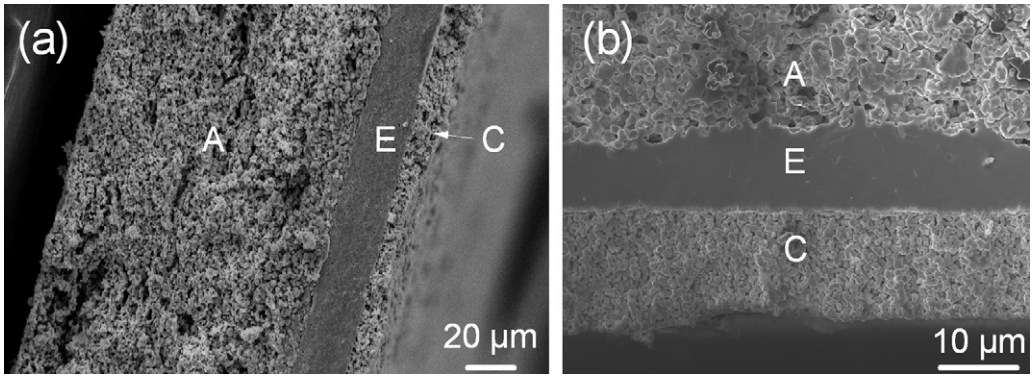

Fig. 4. *Post-mortem* SEM observations of the cells: (a) A and (b) B.

Table 1
Characteristics of the cells recorded at 700 °C: OCV, $P_{0.7\,V}$, extrapolated P_{max}, $ASR_{(U/J)}$ calculated from *U/J* curves, $ASR_{(EIS)}$, R_s and R_p obtained from the EIS measurements and electrolyte thickness obtained from the SEM images.

Cell	OCV (V)	$P_{0.7\,V}$ (mW cm^{-2})	Extr. P_{max} (mW cm^{-2})	$ASR_{(U/J)}$ (0–0.5 A cm^{-2}) (Ω cm^2)	$ASR_{(EIS)}$ (0 A cm^{-2}) (Ω cm^2)	R_s (Ω cm^2)	R_p (Ω cm^2)	Electrolyte thickness t (µm)
A	0.97	209	266	0.87	0.91	0.53	0.38	23
B	1.00	336	398	0.63	0.68	0.30	0.38	11

Table 2
Anode support SOFCs performance from the literature.

Anode	Electrolyte	Cathode	OCV (V)	P_{max} (mW cm^{-2})	ASR (Ω cm^2)	Ref
Ni-YSZ	YSZ (e < 10 µm)	Pd + LSM/YSZ	–	1150 (700 °C)	–	[20]
Ni/GDC ($Ce_{0.8}Gd_{0.2}O_{2-\delta}$)	LSGM ($La_{0.9}Sr_{0.1}Mg_{0.8}Ga_{0.2}\ O_{3-\delta}$) ($e \approx 20$ µm)	SSC ($Sm_{0.5}Sr_{0.5}CoO_{3-\delta}$)	1.1	930 (700 °C)	0.35	[21]
Ni-GDC ($Ce_{0.9}Gd_{0.1}O_{1.95}$)	GDC ($e \approx 40$ µm)	LSCF ($La_{0.8}Sr_{0.2}Co_{0.8}Fe_{0.2}O_3$)	0.935	713 (650 °C)	0.58	[22]
Ni-SDC ($Sm_{0.2}Ce_{0.8}O_{1.9}$)	SDC ($e \approx 20$ µm)	PrBC ($PrBaCo_2O_{5+\delta}$)	0.82	740 (650 °C)	0.13 and 0.33[a]	[23]

[a] The slope of the *U/J* curve evolves with the current density thus two domains can be distinguished and two ASR values have been calculated: the first one for J < 1.2 A cm^{-2} and the second one for J > 1.2 A cm^{-2}.

Table 3
Characteristics of the cell B recorded at 700 °C for different time: OCV, $P_{0.7\,V}$, calculated P_{max}, $ASR_{(U/J)}$.

Time (h)	OCV (V)	$P_{0.7\,V}$ (mW cm^{-2})	Extr. P_{max} (mW cm^{-2})	$ASR_{(U/J)}$ (Ω cm^2)	ASR variation rate (% h^{-1})
0	1.00	336	396	0.64	–
26	0.98	263	316	0.76	0.72
43	0.96	196	251	0.91	0.98
67	0.96	165	212	1.08	1.03
92	0.92	109	151	1.40	1.29

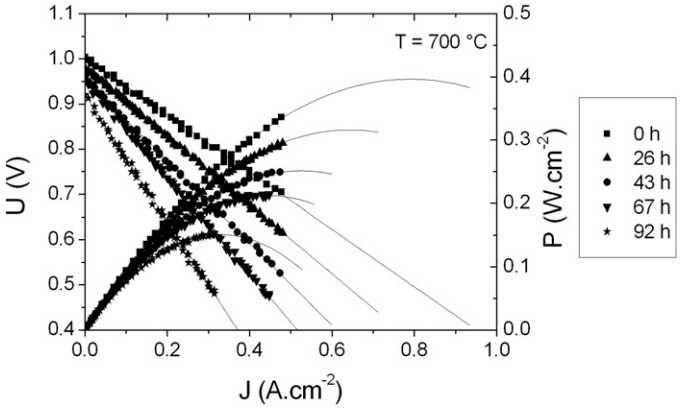

Fig. 5. Voltage and power density versus current density characteristics of the cell B recorded at 700 °C under wet (3% H_2O) hydrogen on the anode side and air on the cathode side for different times, at t = ■, 0 h; ▲, 26 h; ●, 43 h; ▼, 67 h; ⋆, 92 h and –, calculated.

Table 3 gathers the cell characteristics at 700 °C obtained at different times.

The ASR variation rate (Table 3) increases with the time over the period of 92 h. In previous studies, the ageing of the cathode has been followed on cathode/electrolyte/cathode symmetrical cells and it has been seen that the ASR increases at a rate of 0.27% h^{-1} for t < 75 h and then at 0.07% h^{-1} for the end the measurement [9]. Concerning the anode/electrolyte/anode symmetrical cell, the ASR exhibited an increase rate of 0.81% h^{-1} for t < 200 h and then at 0.22% h^{-1} for the end the measurement, attributed to nickel coarsening [7]. For the time period considered (92 h), the combined ageing rates observed separately on the anode and the cathode could be in agreement, with the ageing rate of the complete cell.

During the test, the OCV decreases with the time from 1 V to 0.92 V at t = 0 h and 92 h, respectively. This could mean that the sealing material is damaged during the measurement and thus that the cathode is more and more in contact with hydrogen atmosphere. It is well known that, under low oxygen partial pressure and high temperature environment, perovskite-type cathodes, such as LSM, LSCF or BSCF can be reduced [31–33]. This could explain the rapid degradation of the cell performance. In order to validate this assumption further *post mortem* investigations of the cathode are necessary. However, the cell undergoes a lot of damage when it is removed from the experimental set-up, since the sealing material has to be broken to free the cell. This makes very difficult the post mortem analysis of the cell.

4. Conclusion

In this study, anode supported cells based on BIT07 as electrolyte, BIT07-Ni as anode and LSCF as cathode have been successfully realised by tape-casting and screen-printing, and tested. The best performance has been obtained for a cell with an electrolyte thickness of 11 μm, it presents an ASR value of about 0.68 Ω cm^2, a power density at 0.7 V of around 336 mW cm^{-2} and an extrapolated maximum power density of about 398 mW cm^{-2} at 700 °C. This study validates BIT07 as a promising electrolyte material for SOFC. It has also been seen that decreasing the electrolyte thickness by a factor 2 (from 23 to 11 μm) leads to an increase of the power density at 0.7 V of 60% (from 209 to 336 mW cm^{-2}). In order to improve further more the cell performance the decrease of the electrolyte thickness down to 2 μm yet maintaining the gas tightness of the electrolyte could be investigated by using other design methods, such as chemical vapour deposition (CVD), electro chemical vapour deposition (ECVD) or physical vapour deposition (PVD), to realise the electrolyte [34]. The addition of current collectors on both the anode and the cathode will also be investigated in order to reduce the series resistance contribution and thus decrease the total ASR of the cell.

It has also been seen that at the working temperature of 700 °C, the cell exhibiting the best performance presents a rapid power decrease with time. It has been seen on both anode and cathode symmetrical cells that the two electrodes present performance degradation with the time. The anode is the cell constituent that ages the fastest, thus the introduction of an anode active layer at the anode/electrolyte interface could be explored to slow down the ageing phenomenon. Indeed, this layer would increase the triple phase boundaries near the electrolyte, allowing to reduce the amount of nickel in the rest of the anode [5] and thus prevent nickel coarsening. The use of another sealing material will also be attempted in order to avoid the OCV decrease and the cathode exposition to a reducing atmosphere.

References

[1] B.C.H. Steele, Nature 400 (1999) 619–621.
[2] E. Ivers-Tiffee, A. Weber, D. Herbstritt, J. Eur. Ceram. Soc. 21 (2001) 1805–1811.
[3] V. Jayaraman, A. Magrez, M. Caldes, O. Joubert, M. Ganne, Y. Piffard, L. Brohan, Solid State Ionics 170 (2004) 17–24.
[4] D. Prakash, T. Delahaye, O. Joubert, M.-T. Caldes, Y. Piffard, J. Power Sources 167 (2007) 111–117.
[5] J.-H. Song, S.-I. Park, J.-H. Lee, H.-S. Kim, J. Mater. Process. Technol. 198 (2008) 414–418.
[6] H. Moon, S.D. Kim, S.H. Hyun, H.S. Kim, Int. J. Hydrogen Energ. 33 (2008) 1758–1768.
[7] M. Letilly, O. Joubert, M. Caldes, A. Le Gal La Salle, Int. J. Hydrogen Energ. (2011), doi:10.1016/j.ijhydene.2011.11.140.
[8] M. Letilly, A. Le Gal La Salle, M. Caldes, M. Marrony, O. Joubert, Fuel Cells 9 (2009) 622–629.
[9] M. Letilly, A. Le Gal La Salle, A. Lachgar, O. Joubert, J. Power Sources 195 (2010) 4779–4784.
[10] Y. Tao, H. Nishino, S. Ashidate, H. Kokubo, M. Watanabe, H. Uchida, Electrochim. Acta 54 (2009) 3309–3315.
[11] C. Torres-Garibay, D. Kovar, J. Power Sources 192 (2009) 396–399.
[12] S. Lee, H.S. Song, S.H. Hyun, J. Kim, J. Moon, J. Power Sources 187 (2009) 74–79.
[13] J. Deseure, L. Dessemond, Y. Bultel, E. Siebert, J. Eur. Ceram. Soc. 25 (2005) 2673–2676.
[14] M. Gaudon, C. Laberty-Robert, F. Ansart, L. Dessemond, P. Stevens, J. Power Sources 133 (2004) 214–222.
[15] C. Torres-Garibay, D. Kovar, A. Manthiram, J. Power Sources 187 (2009) 480–486.
[16] F. Tietz, Ionics 5 (1999) 129–139.
[17] M. Letilly, O. Joubert, A. Le Gal La Salle, J. Power Sources, submitted for publication.
[18] Q.-A. Huang, R. Hui, B. Wang, J. Zhang, Electrochim. Acta 52 (2007) 8144–8164.
[19] D. Johnson, ZView:, A Software Program for IES Analysis, Version 2.8, Scribner Associates, Inc., Southern Pines, NC, 2002.
[20] F. Liang, J. Chen, S.P. Jiang, B. Chi, J. Pu, L. Jian, Electrochem. Commun. 11 (2009) 1048–1051.
[21] J.H. Joo, D.Y. Kim, G.M. Choi, Electrochem. Solid State 12 (2009) B65–B68.
[22] C. Ding, H. Lin, K. Sato, T. Hashida, Scr. Mater. 60 (2009) 254–256.
[23] D. Chen, R. Ran, K. Zhang, J. Wang, Z. Shao, J. Power Sources 188 (2009) 96–105.
[24] M.C. Tucker, L. Cheng, L.C. DeJonghe, J. Power Sources 196 (2011) 8313–8322.
[25] M. Guillodo, P. Vernoux, J. Fouletier, Solid State Ionics 127 (2000) 99–107.
[26] S.P. Jiang, J.G. Love, L. Apateanu, Solid State Ionics 160 (2003) 15–26.
[27] S.J. Skinner, Fuel Cells Bull. 4 (2001) 6–12.
[28] J. Hayd, L. Dieterle, U. Guntow, D. Gerthsen, E. Ivers-Tiffée, J. Power Sources 196 (2011) 7263–7270.
[29] K. Kanawka, M.H.D. Othman, Z. Wu, N. Droushiotis, G. Kelsall, K. Li, Electrochem. Commun. 13 (2011) 93–95.
[30] X.-Z. Fu, J. Melnik, Q.-X. Low, J.-L. Luo, K.T. Chuang, A.R. Sanger, Q.-M. Yang, Int. J Hydrogen Energ. 35 (2010) 11180–11187.
[31] T. Nakamura, G. Petrow, L.J. Gauckler, Mater. Res. Bull. 14 (1979) 649–659.
[32] D. Waller, L.G. Coccia, J.A. Kilner, I.W. Boyd, Solid State Ionics 134 (2000) 119–125.
[33] J. Ovenstone, J.-I. Jung, J.S. White, D.D. Edwards, S.T. Misture, J. Solid State Chem. 181 (2008) 576–586.
[34] Z. Liu, M.F. Han, Z. Lei, Key Eng. Mater. 368–372 (2008) 287–289.